Curr Transpl Rep (2016) 3:82–92
DOI 10.1007/s40472-016-0085-x

TISSUE ENGINEERING AND REGENERATION (JA WERTHEIM, SECTION EDITOR)

A Role for 3D Printing in Kidney-on-a-Chip Platforms

Ryan D. Sochol[1] · **Navin R. Gupta**[2] · **Joseph V. Bonventre**[2,3]

Published online: 20 January 2016

Abstract The advancement of "kidney-on-a-chip" platforms—submillimeter-scale fluidic systems designed to recapitulate renal functions in vitro—directly impacts a wide range of biomedical fields, including drug screening, cell and tissue engineering, toxicity testing, and disease modeling. To fabricate kidney-on-a-chip technologies, researchers have primarily adapted traditional micromachining techniques that are rooted in the integrated circuit industry; hence the term "chip." A significant challenge, however, is that such methods are inherently monolithic, which limits one's ability to accurately recreate the geometric and architectural complexity of the kidney in vivo. Better reproduction of the anatomical complexity of the kidney will allow for more instructive modeling of physiological and pathophysiological events. Emerging additive manufacturing or "three-dimensional (3D) printing" techniques could provide a promising alternative to conventional methodologies. In this article, we discuss recent progress in the development of both kidney-on-a-chip platforms and state-of-the-art submillimeter-scale 3D printing methods, with a focus on biophysical and architectural capabilities. Lastly, we examine the potential for 3D printing-based approaches to extend the efficacy of kidney-on-a-chip systems.

Keywords 3D Printing · Kidney-on-a-chip · Organ-on-a-chip · Bioartificial kidney · Additive manufacturing · Microfluidics

This article is part of the Topical Collection on *Tissue Engineering and Regeneration*

✉ Ryan D. Sochol
rsochol@umd.edu

Navin R. Gupta
ngupta12@partners.org

Joseph V. Bonventre
joseph_bonventre@hms.harvard.edu

[1] Department of Mechanical Engineering, Fischell Department of Bioengineering, University of Maryland, 2147 Glenn L. Martin Hall, Building 088, College Park, MD 20742, USA

[2] Renal Division, Brigham and Women's Hospital, Department of Medicine, Harvard Institutes of Medicine, Harvard Medical School, Room 550, 4 Blackfan Circle, Boston, MA 02115, USA

[3] Harvard Stem Cell Institute, Cambridge, MA, USA

Introduction

Although the human kidney is characterized by significant biophysical, architectural, and physiological complexity, two-dimensional (2D) models with quasi-static fluidic conditions represent the predominant method by which kidney cell functions have been investigated in vitro. In recent years, researchers have made considerable efforts to mimic key features of in vivo organ systems in order to promote biologically relevant cell and/or tissue-level behavior in vitro [1]. Through the use of bioengineered microfluidic cell culture platforms—a class of microdevices termed "organ-on-a-chip"—researchers have developed controlled microenvironments, which, coupled with compartmentalization, provide an in vitro means of simulating a number of in vivo chemical, mechanical, and structural factors [2]. Rather than recreating entire organ systems, such platforms consist of the minimal cell or tissue interactions required to model specific functions of a representative organ [3]. For example, "kidney-on-a-chip" platforms typically comprise a singular monolayer of kidney epithelial cells within a microfluidic compartment designed to

reproduce physiologic levels of fluidic shear stress [4]. One caveat to using monolithic microfabrication methods to construct kidney-on-a-chip (and organ-on-a-chip) systems is that the geometric/architectural versatility is inherently limited [5]. Thus, prior efforts have focused on mimicking organ processes in the absence of 3D physiologic structures [6]. A critical uncertainty associated with planar models, however, is the potential impact of multiple scales of kidney architecture (e.g., local and global tubule curvature, tubule-tubule, tubule-interstitial, and tubule-vasculature interactions, etc.) on cell and tissue functionalities [7]. To investigate such fundamental biological questions, new in vitro methodologies are required to better mimic the biological architectures of in vivo renal systems. In particular, emerging 3D printing technologies that afford submillimeter and submicron-scale precision offer distinctive potential for the development of kidney-on-a-chip platforms [8]. In this manuscript, we describe the state of the art for kidney-on-a-chip and 3D printing technologies, and future directions in which the two approaches intersect.

Organ-on-a-Chip Platforms

The development of microfluidic systems for cell and tissue culture has traditionally relied on micromachining technologies [9]. Microscale domains provide considerable scaling-induced benefits for biological applications, including rapid diffusion times [10], low reagent volumes [11], laminar flow profiles [12], precision cell handling [13, 14], high control of microenvironmental conditions [15], and biologically relevant length scales [16–18]. At present, microfluidic devices are predominantly constructed using a technique known as "soft lithography" [19]. Extending prior elastomeric microreplication methods [20], Duffy and Whitesides et al. introduced a protocol for fabricating enclosed microchannels using the silicone elastomer, poly(dimethylsiloxane) (PDMS) [21]. Generally, single-layer microfluidic device manufacturing via soft lithography consists of six key steps: (i) photoresist is spin-coated onto a silicon wafer, (ii) microfeatures are photolithographically defined, (iii) the photoresist is chemically developed, which removes undesired photoresist, (iv) uncured PDMS is poured onto the developed wafer, which serves as a negative master, (v) after curing, the molded PDMS is removed, and individual devices are manually cut and punched with inlet/outlet ports, and (vi) PDMS devices are bonded to substrates (e.g., PDMS or glass) [22–24]. This protocol can be adapted or repeated to construct microfluidic devices with multiple layers and/or levels—a process termed "multilayer soft lithography" [25, 26]. In addition, porous membranes can be incorporated into multilayer systems to promote interactions between separate compartments [27]. These methodologies have served as a fundamental basis for the majority of current organ-on-a-chip platforms.

Although a variety of microfluidic approaches were initially created to model organ systems in vitro, such as the liver [28–32] and lung [33], a critical point in the evolution of organ-on-a-chip technologies was the introduction of a multilayer soft lithography-based "lung-on-a-chip" by Huh and Ingber et al. [34]. To fabricate the system, first, a thin PDMS layer is punched with holes to serve as a porous membrane [34–36]. Thereafter, two micromolded PDMS layers—each with three recessed microchannels—are bonded on opposite sides of the porous PDMS membrane. Lastly, the membrane is selectively etched in the side channels, resulting in a system with (i) two side chambers and (ii) an upper and lower chamber separated by the remaining porous membrane. Although the fabrication protocol is relatively time and labor-intensive, this lung-on-a-chip architecture provides several advantages for biological studies [34–36]. In particular, two distinct cell monolayers can be co-cultured on opposite sides of the intervening porous membrane to reconstitute physiologic tissue-tissue interfaces [33, 34]. Due to the compartmentalized microchannels, the upper and lower chambers can be infused with different fluids (e.g., cell media or air) to apply fluidic shear stress and deliver biomolecules, suspended cells, and/or drug candidates to cell monolayers independently [33–36]. In addition, vacuum can be applied to the side chambers to induce elastic deformation (i.e., physical stretching) of the porous membrane, thereby stimulating seeded cells with substrate-based mechanical cues [34–36]. For the lung-on-a-chip device, cyclical vacuum loading (and therefore, cyclical mechanical strain) was applied to the modeled alveolar-capillary membrane interface to recreate physiologic breathing movements [34, 35].

The lung-on-a-chip methodology has been modified to model additional organ functions, such as the peristaltic motions of the human intestine [37, 38]. Additionally, many groups have also utilized multilayer, membrane-based methodologies [27, 33] to examine a number of other physiological systems, such as the blood-brain barrier [39–41] and bone marrow [42]. In particular, investigators have designed a wide range of microfluidic platforms to recapitulate renal functions in vitro [43, 44, 45••, 46–48].

Kidney-on-a-Chip

The ability to accurately identify nephrotoxic agents during the pre-clinical testing stage would enable earlier discontinuation of drug development with a particular therapeutic agent and modification to maintain efficacy with less or no kidney toxicity [49–51]. Early recognition likely will reduce the nearly 20 % of nephrotoxicity-based drug attrition in phase 3 clinical trials, saving substantial development time and cost [52]. For disease modeling, enhanced precision and experimental controls associated with in vitro testing could enable new

insights into kidney disease mechanisms, while providing a promising means to screen new therapies [53, 54]. Consequently, investigators have focused on developing improved in vitro models that will mimic cellular responses in vivo and retain renal cellular functionalities. During drug discovery, the industry standard for pre-clinical screening remains toxicity testing of 2D human cell cultures under quasi-static fluidic conditions, such as in petri dishes and multiwell plates (Fig. 1a). Despite their predominance, such testing methods lack critical microenvironmental stimuli to effectively mimic in vivo conditions [55].

At present, the majority of kidney-on-a-chip platforms rely on three primary architectures: (i) single-layer microfluidic systems (Fig. 1b), (ii) multilayer microfluidic systems comprised of two chambers separated by a permeable membrane (Fig. 1c), and (iii) systems comprised of a singular, straight tubular structure (Fig. 1d). These device designs have enabled researchers to investigate and reconstitute several functions of separate nephron segments (Table 1).

Single-Layer Microfluidic Systems

Compared to their multilayer counterparts, single-layer microfluidic devices (Fig. 1b) benefit from lower manufacturing costs, time, and labor, which have made such systems attractive for cellular studies. To model kidney epithelial cells, Huang and Wu et al. created a single-layer microfluidic system for co-culturing Madin-Darby canine kidney (MDCK) epithelial cells with collagen gel-embedded adipose stem cells (ASCs) [56]. There was a 35 % increase in cellular height (with columnar shape), promotion of cilia formation, and increased Na/K ATPase expression [56]. It should be recognized, however, that MDCK cells have characteristics of the distal nephron, which make up a much smaller part of the tubule than does the proximal tubule (which comprises approximately 90 % of the mass of the kidney cortex). Zhou, Lin, and Qin et al. developed a single-layer architecture to replicate proteinuric nephropathy and investigate changes in immortalized proximal tubular epithelial cells (HK-2) where they express characteristics of mesenchymal cells and become dedifferentiated - behavior often associated with renal interstitial fibrosis [57]. In response to serum proteins and C3a alone, HK-2 cells either underwent apoptosis or adopted a mesenchymal phenotype; however, such effects were not observed in response to heat-inactivated serum [57]. Frohlich, Zhang, and Charest adapted the single-layer approach by modifying the bottom substrate with microgrooves aligned in the direction of microfluidic flow [58]. The combination of surface topography and fluidic shear stress not only promoted cell alignment in the direction of the groove lines and flow, but also enhanced tight junction formation for seeded HK-2 cells [58]. In general, improved physiologic behavior of kidney cells in response to applied fluidic shear stress was consistently found by multiple groups in many experiments [56–58].

Multilayer Microfluidic Systems

One of the first multilayer microfluidic devices to be used for modeling renal functions was published by Jang and Suh [43]. Designed to recapitulate functions of the collecting duct, the

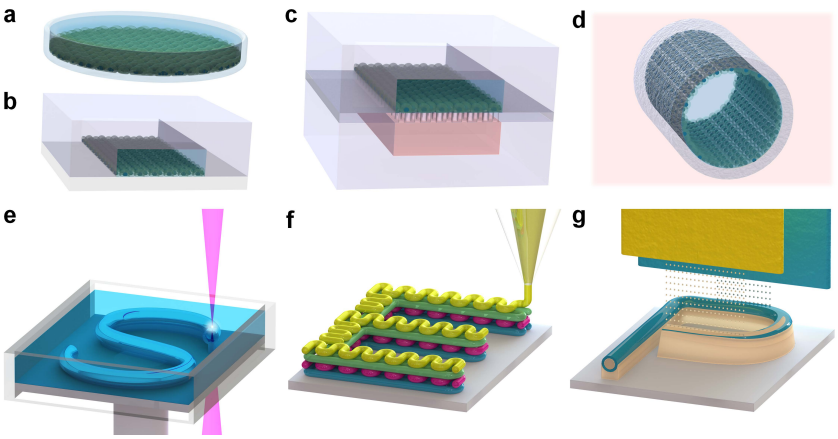

Fig. 1 Conceptual illustrations of (**a**–**d**) kidney epithelial cell testing platform architectures and (**e**–**g**) 3D printing approaches. **a** Petri dish with a 2D cell monolayer under quasi-static fluidic conditions. **b** Single-layer microfluidic system with a 2D cell monolayer. Fluidic shear stress can be applied to cells seeded in the microchannel. **c** Multilayer microfluidic system with a 2D cell monolayer on an intervening porous membrane. Fluidic shear stress can be applied to cells seeded in the upper chamber, with quasi-static fluid in the lower chamber to represent the interstitial space. **d** Tubular porous membrane with a 3D cell monolayer. Fluidic shear stress can be applied to cells seeded within the tubular membrane, with quasi-static fluid outside to represent the interstitial space. **e** Stereolithography (SLA). Focused light induces localized photopolymerization (*white*) of a photocurable material (*blue*) to fabricate 3D structures. **f** Extrusion-based printing. Material is extruded through a nozzle and deposited to fabricate 3D structures. **g** PolyJet Printing (PJP)/ MultiJet Modeling (MJM). Multiple inkjets in parallel deposit microdroplets of photocurable material and sacrificial support material simultaneously to fabricate 3D structures

platform included a thin polyester membrane sandwiched between an enclosed upper PDMS microchannel and a lower PDMS well exposed to static media in a 35-mm culture dish. Fluidic shear stress applied to MDCK cells (seeded in the upper chamber on the 2D porous membrane) induced cell polarity, as evidenced by the expression of the apical water channel protein, aquaporin-2 (AQP2), and basolateral Na/K ATPase. Immunohistochemical staining confirmed that fluidic shear stress prompted improved cytoskeletal reorganization, focal adhesions, and cell junctions. Similar to in vivo physiology, the addition of vasopressin to the basolateral channel resulted in increased apical chamber osmolarity. Furthermore, the addition of aldosterone to the basolateral channel resulted in decreased sodium concentration sampled in the apical chamber [43]. Due to heterogeneity and limitations intrinsic to MDCK cell populations [59], Jang and Suh et al. applied a structurally identical device to investigate the behavior of rat primary inner medullary collecting duct (IMCD) cells [44]. Apical AQP2 trafficking was associated with vasopressin-induced F-actin depolymerization; however, in the absence of vasopressin, fluidic shear stress alone induced F-actin depolymerization and AQP2 translocation [44].

Subsequent models have focused primarily on the proximal tubule [45••, 46–48]. In a functional nephron, numerous filtered substances in the intraluminal compartment require reabsorption, while various substances retained in the bloodstream require secretion into the lumen. Armed with solute selective transporters and AQP1 water channels on the apical membrane, the proximal tubule iso-osmotically reabsorbs 65 % of water, sodium, and chloride, 90 % of bicarbonate, and 100 % of glucose and amino acids from the glomerular filtrate [60]. Basolateral influx of organic acids and bases, via organic anion transporters (OATs) and organic cation transporters (OCTs) coupled to apical efflux through the multidrug resistance 1 (MDR1) gene product p-glygoprotein 1 (Pgp), allowed for the excretion of xenobiotics and exogenous toxins. To model a number of these functions, Jang, Ingber and colleagues further adapted the aforementioned multilayer approach to create a proximal tubule-on-a-chip for drug toxicity testing using HK-2 cells [45••]. Proximal tubular toxicity to cisplatin—a known OCT2 ligand—was replicated and reversed with cimetidine—a known OCT2 inhibitor. Applied fluidic shear stress resulted in increased Pgp-mediated efflux, cell polarity, cilia expression, brush-border alkaline phosphatase activity, and albumin and glucose resorption [45••]. Using a similar multilayer, membrane-based architecture with an enclosed bottom channel (Fig. 1c), Sciancalepore and Pisignano et al. cultured adult renal stem/progenitor cells (ARPCs) to model the proximal tubule [46]. The system included a porous polycarbonate membrane sandwiched between two identical PDMS microchannels. Consistent with prior work, applied fluidic shear stress promoted apical and basolateral localization of the AQP2 transporter and Na/K ATPase pump, respectively [46].

To model the renal reabsorptive barrier, Frohlich, Charest, and colleagues adapted their prior methodology [58] to achieve a multilayer device with a topographically patterned porous polycarbonate membrane [47]. Consistent with the previous results [58], HK-2 cells and primary renal proximal tubule epithelial cells (RPTECs) aligned in the direction of the groove lines [47]. Another multilayer system by Ferrell, Fissell, and colleagues included the integration of electrodes to measure the transepithelial electrical resistance (TEER) and assess cell junction integrity for both MDCK cells and RPTECs [48]. In response to applied fluidic shear stress, RPTECs revealed phenotypic changes, including disassembly of cytosolic F-actin stress fibers [48].

Tubular Microfluidic Systems

In contrast to the aforementioned planar approaches, researchers have also explored new methodologies to better account for the local microcurvatures of in vivo kidney tubules. Wei, Nei, Bandyopadhyay, and colleagues developed a microfluidic device with a single, cylindrical microchannel by (i) fabricating a straight, rectangular microchannel and then (ii) executing a sol-gel-based protocol [61] for coating PDMS microchannels with glass approximately ten times in succession to resolve a circular channel cross-section [62•]. The transition to a circular microchannel enabled HK-2 cells to be seeded uniformly on the cylindrical walls, similar to in vivo physiology. The device lumen was subjected to increasing concentrations of calcium, resulting in a calcium phosphate product that was at supersaturation, and a demonstration of real-time calcium phosphate stone production within the tubular microfluidic platform [62•]. One drawback inherent to the glass-coated device, however, is that in vivo-like transport phenomena from the lumen to the interstitial space (e.g., those demonstrated with membrane-based systems [43, 44, 45••, 46–48]) could not be recapitulated [62•]. An alternative method to bypass this issue is the use of hollow tubular membranes (Fig. 1d), such as those presented by Oo, Ying, Zink, and colleagues [63•]. In particular, Ng et al. designed a bioartificial kidney device in which a straight, tubular hollow-fiber membrane was embedded within a multicompartment microfluidic system [64]. The device architecture enabled fluid flow inside and outside the tubular membrane to be accessed independently. For cellular testing, the hollow tubular membranes were allowed to absorb bovine fibrinogen and perfused with bovine thrombin. Subsequent fibrin products cross-linked to form a sacrificial extracellular matrix (ECM), which supported the seeding of RPTECs. Experimental results demonstrated that inulin recovery could be used as a surrogate for the generation of a confluent monolayer of cells, as inulin moves across the cell layer in a paracellular fashion in regions without

Table 1 Notable kidney-on-a-chip platforms

Author	Date	Cell type	Cell line(s)	Device type	Device design characteristics and materials
Huang et al. [56]	2013	Proximal/distal tubule	MDCK, CG-ASC	B	$h = 150$ μm, $w = 2$–3 mm; PDMS, glass
Zhou et al. [57]	2014	Proximal tubule	HK-2	B	$h = 100$–150 μm, $w = 800$–1000 μm, $l = 1.5$–2.2 mm; PDMS, glass
Frolich et al. [58]	2012	Proximal tubule	HK-2	B	$h = 150$ μm, $w = 3$ mm, $l = 18$ mm; grooves = 0.75 μm × 0.75 μm; polystyrene, PDMS
Jang et al. [43, 44]	2010, 2011	Collecting duct	MDCK, IMCD	C	$h = 100$ μm, $w = 1$–2 mm, $l = 6$–10 mm; PDMS; Membrane $t = 10$ μm, $p = 0.4$ μm; polyester
Jang et al. [45••]	2013	Proximal tubule	RPTEC	C	$h = 100$ μm, $w = 1$–1.1 mm, $l = 10$-11 mm; PDMS; Membrane $t = 10$ μm, $p = 0.4$ μm; polyester
Sciancalepore et al. [46]	2014	Proximal tubule	ARPC	C	$h = 120$ μm, $w = 500$ μm; PDMS Membrane $t = 40$ μm, $p = 0.1$ μm; polyester
Frohlich et al. [47]	2013	Proximal tubule	RPTEC, HK-2	C	$h = 75$–100 μm, $w = 250$–350 μm; grooves = 0.5–1 μm × 0.75 μm; PDMS; Membrane $t = 5$–10 μm, $p = 3$–12 μm; polycarbonate
Ferrell et al. [48]	2010	Proximal tubule	RPTEC	C	$h = 50$ μm, $w = 3.1$ mm, $l = 43$ mm; PDMS; Membrane $t = 10$ μm, $p = 1$ μm; polycarbonate
Wei et al. [62•]	2012	Proximal tubule	HK-2	B/D	$D = 400$ μm, $l = 30$ mm; glass, PDMS
Oo et al. [63•]	2011	Proximal tubule	RPTEC	D	$D = 500$ μm, $l = 25$ mm, $t = 145$ μm, $p \leq 0.5$ μm; PES/PVP
Ng et al. [64]	2013	Proximal tubule	RPTEC	D	$D = 500$ μm, $l = 25$ mm; $t = 145$ μm, $p \leq 0.5$ μm; PES/PVP, PDMS, glass

MDCK Madin-Darby canine kidney, *CG-ASC* collagen gel encapsulated adipose stem cell (canine), *IMCD* inner medullary collecting duct (rat), *RPTEC* primary renal proximal tubular epithelial cell (human), *ARPC* adult renal progenitor cell (human), *PDMS* poly(dimethylsiloxane), *PES*/*PVP* polyethersulfone/polyvinylpyrrolidone

h = channel height

w = channel width

l = channel length

t = membrane thickness

p = membrane pore size

appropriate tight junctions [64]. Additional extensions of tubular kidney platforms that enable researchers to recreate local variations in tubule geometry (e.g., diameter and shape), global changes in tubule architecture (e.g., tortuosity), and tubule-tubule and/or tubulo-vascular interfaces could further improve the biomimetic efficacy of in vitro approaches for modeling renal physiology.

Submillimeter-Scale 3D Printing

Although traditional methods of microdevice construction (e.g., soft lithography) afford significant benefits in terms of microscale precision and optical transparency, limitations inherent to such protocols remain a ubiquitous problem for biological applications [65]. A critical barrier for investigators outside of engineering fields is that gaining access to microfabrication facilities is often difficult and may require considerable technical training and high usage fees [66]. Furthermore, the clean room-based procedures for wafer processing are typically executed manually and can be exceedingly cost, time, and labor-intensive [67]. These issues are exacerbated when fabricating multilayer device designs that require distinct layers to be aligned and assembled manually [68]. The most crucial drawback for modeling in vivo physiology is that the monolithic restriction renders non-planar physical structures difficult or impossible to reconstitute via conventional micromachining processes. Consequently, alternative manufacturing methods capable of bypassing the aforementioned limitations could offer significant promise for diverse biological studies and applications.

Additive manufacturing—widely referred to as 3D printing—encompasses a number of methods for building 3D structures through point-by-point (PbP) and/or layer-by-layer (LbL) processes. Generally, computer-aided design (CAD) tools are used to generate a digital 3D model, which is then sent to a 3D printer for autonomous device construction. The

first 3D printing technique—stereolithography (SLA), which was introduced by Hull—involves using a bath of liquid-phase photoreactive material and a focused light beam to photocure (i.e., solidify) the material PbP, LbL, to ultimately fabricate a 3D object comprised of cured material (Fig. 1e) [69]. Subsequently, Crump described an extrusion-based method in which a dispensing head or nozzle is used to directly deposit material PbP, LbL, to form 3D constructs (Fig. 1f) [70]. Yamane et al. created a technique for building 3D structures by inkjet printing a photosetting or thermosetting material LbL [71], which combined with the simultaneous printing of a sacrificial support material [72], became the basis for 3D printing technologies including MultiJet Modeling (MJM) and PolyJet Printing (PJP) (Fig. 1g). Although researchers have developed numerous 3D manufacturing methodologies for applications throughout broad academic and industrial fields, the submillimeter-scale 3D printing techniques with characteristics relevant to kidney-on-a-chip systems stem from three fundamental approaches: (i) SLA, (ii) extrusion-based printing, and (iii) PJP/MJM (Table 2).

Stereolithography-Based Microsystems

One of the first steps toward 3D printed microfluidics was the use of SLA processes to direct-write structures within prefabricated, single-layer PDMS microfluidic channels [73, 74]. By loading photocurable material into microfluidic channels, complex geometric structures can be photocured in situ to facilitate improved mixing dynamics [73] and multidirectional fluidic vias [74]. In recent years, however, researchers have utilized SLA to construct entire microfluidic systems [75–79]. For example, Shallan and Breadmore et al. demonstrated 3D microfluidic gradient and microdroplet generators constructed by means of digital-mirror device (DMD), projection-based SLA [75]. Au, Lee, and Folch evaluated the resolution of mail-order SLA-based microfluidic devices with rectangular microchannels and successfully cultured and imaged Chinese hamster ovary (CHO-K1) cells within the microfluidic devices [77]. Using similar SLA methods, Bhargava and Malmstadt et al. developed a number of discrete and reconfigurable elements consisting of microchannels with varying lengths (and therefore, resistances), which were utilized for microfluidic applications including mixing and droplet generation [76]. Subsequently, Au et al. presented 3D printed microfluidic systems with moving valves and pumps, which were employed to create a multi-fluid perfusion chamber for CHO-K1 cells [78].

In addition to constructing microfluidic systems, SLA can be used to build 3D cellular scaffolds. In particular, the Chen group has developed DMD-based continuous-projection SLA methods for creating hydrogel scaffolds for a variety of cellular studies [80–82]. Zhang et al. constructed 3D microstructured scaffolds and microwells using photocurable poly(ethylene glycol) diacrylate (PEGDA) and gelatin methacrylate (GelMA) materials [80]. Both human umbilical vein endothelial cells (HUVECs) and NIH-3T3 mouse embryonic fibroblast cells (3T3s) were cultured on the 3D scaffolds. Both cell types exhibited distinct morphology, and in some cases, multicellular structure, when grown on curvature when compared to 2D substrates [80]. Soman et al. constructed PEGDA-based "log-pile" microarchitectures with varying mechanical stiffness to investigate the impact of mechanical stimuli on 3D motility of normal human mammary epithelial (HMLE) cells and cancerous, twist-transformed (HMLET) cells [81]. Using their well-printing methodology [80], Hribar et al. built concave PEGDA microwells to culture BT474 breast cancer cell spheroids and induced pluripotent stem cell (iPSC) embryoid bodies (EBs) [82]. In response to microwell curvature, the iPSC EBs exhibited decreased polydispersity in size and maintained an undifferentiated state for an extended time, revealing potential roles of microscale geometry in iPSC functions [82].

An extension of SLA in which multiphoton absorption is used for spatially controlled photopolymerization has enabled 3D manufacturing with resolutions down to the 100 nm range [83]. This technique—referred to as direct laser writing (DLW)—has been applied to create geometrically complex 3D cellular scaffolds [84, 85•, 86]. Using Ormocomp photoresist, Klein, Wegener, and Bastmeyer et al. applied DLW to construct web-like elastic scaffolds to measure the traction forces of seeded primary chicken embryonic cardiomyocytes (CECs) [84]. To control the formation of cell adhesion sites (and therefore, cell shape) for primary chicken embryonic fibroblasts (CEFs), the same group executed the DLW process twice in succession to create 3D composite-polymer scaffolds comprised of both Ormocomp and PEGDA to promote or prevent cell attachment, respectively [85•, 86]. To date, DLW has resulted in the finest resolutions for 3D cellular scaffold printing; however, this also limits the overall build size to the submillimeter range [84, 85•, 86]. One additional condition of note for SLA-based methods is that successful printing of many 3D designs requires the inclusion of fully integrated support structures (e.g., pillar-like ribs), which can be challenging or unfeasible to remove following the 3D printing process [87].

Extrusion-Based Microsystems

The use of extrusion-based techniques for 3D "bioprinting" primarily revolves around the deposition of either sacrificial materials, such as fugitive inks, or cell-compatible materials, such as cell-laden gels. The Lewis group has pioneered a number of fugitive ink-based methods for resolving complex 3D microfluidic systems. To construct 3D vascular-inspired networks, Therriault et al. presented a four-step protocol: (i)

Table 2 Notable 3D printed microfluidic systems and/or cellular constructs

Authors	Date	3D printing method	System type	Resolution (μm)	3D printed material	Cell type
Shallan et al. [75]	2014	SLA (DMD)	Microfluidic	500–1000	Proprietary resin	N/A
Bhargava et al. [76]	2014	SLA	Microfluidic	500–1000	WaterShed XC 11122	N/A
Au et al. [77, 78]	2014, 2015	SLA	Microfluidic, cell scaffold	100–400	WaterShed XC 11122	CHO-K1
Zhang et al. [80]	2012	SLA (DMD)	Cell scaffold	10–100	PEGDA, GelMA	3T3, HUVEC
Soman et al. [81]	2012	SLA (DMD)	Cell scaffold	10–100	PEGDA	HMLE, HMLET
Hribar et al. [82]	2015	SLA (DMD)	Cell scaffold	10–100	PEGDA	BT474, iPSC
Klein et al. [84, 85•]	2010, 2011	SLA (DLW)	Cell scaffold	0.1–0.5	Ormocomp, PEGDA	CEC, CEF
Scheiwe et al. [86]	2015	SLA (DLW)	Cell scaffold	0.1–0.5	Ormocomp, PEGDA	CEF
Therriault et al. [88]	2003	Extrusion (sacrificial)	Microfluidic	10–300	Prussian blue paste	N/A
Wu et al. [90]	2011	Extrusion (sacrificial, omnidirectional)	Microfluidic	10–200	Pluronic F127	N/A
Miller et al. [91]	2012	Extrusion (sacrificial)	Microfluidic, cell scaffold	150–750	Carbohydrate glass	HUVEC, 10T1/2, 3T3, HEK 293T, rat hepatocyte
Rutz et al. [94]	2015	Extrusion (cell-laden)	Cell construct	350–1300	PEG SVA, GelMA	HUVEC, HDF, hMSC
Kolesky et al. [96••]	2014	Extrusion (sacrifical and cell-laden)	Microfluidic, cell scaffold	45–500	Pluronic F127, GelMA	HUVEC, 10T1/2, HNDF
Gao et al. [95]	2015	Extrusion (sacrifical and cell-laden)	Microfluidic, cell scaffold	600–1500	Calcium alginate	L929 mouse fibroblasts
Anderson et al. [97]	2013	PJP	Millifluidic (+ insert)	100	Objet Vero White Plus	BPAE
Lee et al. [98]	2014	MJM	Microfluidic	35–100	VisiJet M3 Crystal	N/A
Zhu et al. [100]	2015	MJM, SLA	Microfluidic, cell trapping	50–100	VisiJet M3 Crystal and SL Clear, WaterShed XC 11122, Dreve Fototec 7150 Clear	Zebrafish embryos

PEGDA poly(ethylene glycol) diacrylate, *GelMA* gelatin methacrylate, *PEG SVA* poly(ethylene glycol) succinimidyl valerate, *HUVEC* human umbilical vein endothelial cells, *HMLE* normal human mammary epithelial cells, *HMLET* twist-transformed human mammary epithelial cells, *iPSC* induced plouripotent stem cells, *CEC* primary chicken embryonic cardiomyocytes, *CEF* primary chicken embryonic fibroblasts, *HDF* human dermal fibroblasts, *hMSC* human mesenchymal stem cells, *HNDF* human neonatal dermal fibroblasts, *BPAE* bovine pulmonary artery endothelial cells, *N/A* not applicable, *CHO-K1* chinese hamster ovary cells, *3T3* NIH-3T3 mouse embryonic fibroblast cells, *BT474* breast cancer cell spheroids, *10T1/2* mouse fibroblasts, *HEK 293T* human embryonic kidney cells

micronozzles are used to 3D print a fugitive organic ink network, (ii) the fugitive ink scaffold is infiltrated with a surrounding liquid resin, (iii) the surrounding resin is cured, and (iv) heat is applied to the fugitive organic ink to enable vacuum-based extraction, thereby leaving behind a 3D network of hollow, interconnected microfluidic channels [88]. Wu et al. adapted this method by using the group's omnidirectional printing technique [89] to extrude free-floating fugitive ink within a reservoir of photopolymerizable hydrogel [90]. Following the printing process, the surrounding hydrogel was photocured, and the liquid-phase fugitive ink was evacuated via applied pressure. The resulting system included vascular-like microfluidic channels within a hydrogel matrix [90]. Using a similar approach, Miller and Chen et al. first printed a sacrificial 3D carbohydrate glass lattice, but instead encapsulated the 3D network with living cells and ECM [91]. The full construct was then placed in cell media, which dissolved the carbohydrate glass filaments, thereby allowing for the remaining fluid to be replaced by fresh medium and/or suspended cells. The resulting scaffold supported viability for HUVECs, 10T1/2 mouse fibroblasts, 3T3s, human embryonic kidney (HEK 293T) cells, and primary rat hepatocytes [91].

Extrusion-based deposition of cell-compatible materials and/or cell-laden gels represents the most widely used approach for 3D bioprinting of cellular constructs [92–95, 96••]. Recently, Rutz and Shah et al. used micronozzles to extrude poly(ethylene glycol) succinimidyl valerate (PEG SVA) and GelMA to 3D print self-supporting cross-hatched structures embedded with HUVECs, human dermal fibroblasts (HDFs), and human mesenchymal stem cells (hMSCs) [94]. Using a coaxial nozzle, Gao and He et al. printed cellular constructs comprised of hollow, cell-laden calcium alginate

filaments that supported internal media flow [95]. One notable recent approach by Kolesky and Lewis et al. involved the integration of both fugitive and cell-laden hydrogel inks to model vascularized, heterogeneous tissue constructs [96••]. Three inks, including one Pluronic F127 fugitive ink and two distinct cell-laden GelMA inks, were 3D printed as free-floating structures within a GelMA reservoir. After evacuating the fugitive ink, the remaining microchannels were endothelialized with HUVECs, resulting in a 3D printed tissue construct that allowed for interactions between 10T1/2 fibroblasts, human neonatal dermal fibroblasts (HNDFs), and HUVECs [96••]. The key limitation inherent to the extrusion-based methodologies is that the materials must be deposited PbP by a physical extruder (e.g., nozzle). As a result, not only does the printing process require comparatively more time, but also fabricating complex geometries can be especially challenging. Nonetheless, no other 3D printing approaches at present have had as much impact on 3D biomanufacturing or enabled as much flexibility in cellular placement, material selection, and heterogeneous cellular interactions as extrusion-based methods.

Polyjet/Multijet Modeling-Based Microsystems

PJP and MJM technologies utilize high numbers of microscale inkjets in parallel to deposit microdroplets of either a photopolymer or a sacrificial support material via a LbL process (with continual curing) to produce 3D objects. After printing completion, the support material can be removed during post-processing. Although these methods provide considerable advantages in terms of resolution, build volumes, print speeds, and sacrificial supports, PJP/MJM material selection remains limited to a very small number of proprietary materials. Due to this lack of material versatility, such methods are not yet well-suited for many cellular applications. An initial work by Anderson and Spence et al. demonstrated that PJP-based millifluidic systems could be used for drug transport studies by first culturing bovine pulmonary artery endothelial (BPAE) cells to confluence on external (non-printed) cell culture membranes, which were then inserted into a designated slot in a 3D printed system [97]. Researchers have also applied MJM technologies to construct fluidic channels with varying geometries [98, 99]. To compare the efficacy of MJM technologies to SLA methods, Zhu and Wlodkowic et al. constructed a number of identical fluidic systems for arraying and imaging zebrafish embryos [100]. Despite successful fluidic trapping performance, the majority of the MJM and SLA resins tested were found toxic and/or caused significant developmental abnormalities over the course of multi-day experiments, with an MJM material, Visijet M3 Crystal, exhibiting the worst performance in terms of biotoxicity [100].

Conclusion

The development of kidney-on-a-chip platforms capable of accurately mimicking the diversity of in vivo environmental conditions and physiological compositions offers significant potential for biomedicine, particularly for better understanding organ biology and establishing structures that can replace function. To accomplish these goals with respect to the kidney, future kidney-on-a-chip systems will require added complexity to simultaneously reconstitute five fundamental tiers of renal physiology: (i) fluidic conditions associated with tubular flow, (ii) cell-matrix interactions associated with tubular microenvironments (e.g., ECM and growth factors), (iii) biophysical characteristics associated with tubular microenvironments, including mechanical stiffness and porosity, (iv) multiscale geometric features of individual kidney tubules, such as local and global microcurvature and size, and (v) cell-cell and tissue-tissue interfaces stemming from the structural organization of discrete kidney tubules adjacent not only to other tubules but also to vasculature and other relevant cell types. This next generation of kidney-on-a-chip devices will demand significant advancements in biomanufacturing methodologies, such as those afforded by emerging micro/nanoscale 3D printing processes. Although individual 3D printing techniques each provide distinct benefits for recreating finite units of physiologic structures and/or functions, no singular method yet encompasses the full array of capabilities required to accurately recapitulate in vivo kidney physiology. Nonetheless, current micro/nanoscale 3D printing approaches offer numerous advantages over traditional microfabrication methodologies, and thus, future research should focus on transitioning toward 3D printed kidney-on-a-chip platforms.

Compliance with Ethical Standards

Conflict of Interest Ryan D. Sochol, Navin R. Gupta, and Joseph V. Bonventre declare that they have no conflict of interest.

Human and Animal Rights and Informed Consent This article does not contain any studies with human or animal subjects performed by any of the authors.

References

Papers of particular interest, published recently, have been highlighted as:
- • Of importance
- •• Of major importance

1. Marx V. Tissue engineering: organs from the lab. Nature. 2015;522(7556):373–7.

2. Bhatia SN, Ingber DE. Microfluidic organs-on-chips. Nat Biotechnol. 2014;32(8):760–72.
3. Esch EW, Bahinski A, Huh D. Organs-on-chips at the frontiers of drug discovery. Nat Rev Drug Discov. 2015;14(4):248–60.
4. Caplin JD, Granados NG, James MR, Montazami R, Hashemi N. Microfluidic organ-on-a-chip technology for advancement of drug development and toxicology. Adv Healthcare Mater. 2015;4(10): 1426–50.
5. Huh D, Torisawa Y-s, Hamilton GA, Kim HJ, Ingber DE. Microengineered physiological biomimicry: organs-on-chips. Lab Chip. 2012;12(12):2156–64.
6. Eisenstein M. Artificial organs: honey, I shrunk the lungs. Nature. 2015;519(7544):S16–8.
7. Fitzgerald KA, Malhotra M, Curtin CM, O' Brien FJ, O' Driscoll CM. Life in 3D is never flat: 3D models to optimise drug delivery. J Control Release. 2015;215:39–54.
8. Murphy SV, Atala A. 3D bioprinting of tissues and organs. Nat Biotechnol. 2014;32(8):773–85.
9. Sackmann EK, Fulton AL, Beebe DJ. The present and future role of microfluidics in biomedical research. Nature. 2014;507(7491): 181–9.
10. Sochol RD, Casavant BP, Dueck ME, Lee LP, Lin L. A dynamic bead-based microarray for parallel DNA detection. J Micromech Microeng. 2011;21(5):054019.
11. Tan WH, Takeuchi S. A trap-and-release integrated microfluidic system for dynamic microarray applications. Proc Natl Acad Sci U S A. 2007;104(4):1146–51.
12. Sochol RD, Lu A, Lei J, Iwai K, Lee LP, Lin L. Microfluidic bead-based diodes with targeted circular microchannels for low Reynolds number applications. Lab Chip. 2014;14(9):1585–94.
13. Tan WH, Takeuchi S. Dynamic microarray system with gentle retrieval mechanism for cell-encapsulating hydrogel beads. Lab Chip. 2008;8(2):259–66.
14. Sochol RD, Li S, Lee LP, Lin L. Continuous flow multi-stage microfluidic reactors via hydrodynamic microparticle railing. Lab Chip. 2012;12:4168–77.
15. Kuribayashi-Shigetomi K, Onoe H, Takeuchi S. Cell Origami. Self-folding of three-dimensional cell-laden microstructures driven by cell traction force. Plos One. 2012;7(12).
16. Tan JL, Tien J, Pirone DM, Gray DS, Bhadriraju K, Chen CS. Cells lying on a bed of microneedles: an approach to isolate mechanical force. Proc Natl Acad Sci U S A. 2003;100(4):1484–9.
17. Sochol RD, Higa AT, Janairo RRR, Li S, Lin L. Unidirectional mechanical cellular stimuli via micropost array gradients. Soft Matter. 2011;7(10):4606–9.
18. Sochol RD, Higa AT, Janairo RRR, Li S, Lin L. Effects of micropost spacing and stiffness on cell motility. Micro Nano Lett. 2011;6(5):323–6.
19. Whitesides GM. The origins and the future of microfluidics. Nature. 2006;442(7101):368–73.
20. Aumiller GD, Chandross EA, Tomlinson WJ, Weber HP. Submicrometer resolution replication of relief patterns for integrated optics. J Appl Phys. 1974;45(10):4557–62.
21. Duffy DC, McDonald JC, Schueller OJA, Whitesides GM. Rapid prototyping of microfluidic systems in poly(dimethylsiloxane). Anal Chem. 1998;70(23):4974–84.
22. McDonald JC, Duffy DC, Anderson JR, Chiu DT, Wu H, Schueller OJA, et al. Fabrication of microfluidic systems in poly(-dimethylsiloxane). ELECTROPHORESIS. 2000;21(1):27–40.
23. Sochol RD, Dueck ME, Li S, Lee LP, Lin L. Hydrodynamic resettability for a microparticle arraying system. Lab Chip. 2012;12:5051–6.
24. Sochol RD, Corbett D, Hesse S, Krieger WER, Wolf KT, Kim M, et al. Dual-mode hydrodynamic railing and arraying of microparticles for multi-stage signal detection in continuous flow biochemical microprocessors. Lab Chip. 2014;14(8):1405–9.
25. Anderson JR, Chiu DT, Jackman RJ, Cherniavskaya O, McDonald JC, Wu H, et al. Fabrication of topologically complex three-dimensional microfluidic systems in PDMS by rapid prototyping. Anal Chem. 2000;72(14):3158–64.
26. Unger MA, Chou HP, Thorsen T, Scherer A, Quake SR. Monolithic microfabricated valves and pumps by multilayer soft lithography. Science. 2000;288(5463):113–6.
27. Ismagilov RF, Ng JMK, Kenis PJA, Whitesides GM. Microfluidic arrays of fluid-fluid diffusional contacts as detection elements and combinatorial tools. Anal Chem. 2001;73(21):5207–13.
28. Allen JW, Bhatia SN. Formation of steady-state oxygen gradients in vitro: application to liver zonation. Biotechnol Bioeng. 2003;82(3):253–62.
29. Viravaidya K, Shuler ML. Incorporation of 3T3-L1 cells to mimic bioaccumulation in a microscale cell culture analog device for toxicity studies. Biotechnol Prog. 2004;20(2):590–7.
30. Kane BJ, Zinner MJ, Yarmush ML, Toner M. Liver-specific functional studies in a microfluidic array of primary mammalian hepatocytes. Anal Chem. 2006;78(13):4291–8.
31. Lee PJ, Hung PJ, Lee LP. An artificial liver sinusoid with a microfluidic endothelial-like barrier for primary hepatocyte culture. Biotechnol Bioeng. 2007;97(5):1340–6.
32. Carraro A, Hsu WM, Kulig KM, Cheung WS, Miller ML, Weinberg EJ, et al. In vitro analysis of a hepatic device with intrinsic microvascular-based channels. Biomed Microdevices. 2008;10(6):795–805.
33. Huh D, Fujioka H, Tung Y-C, Futai N, Paine R, Grotberg JB, et al. Acoustically detectable cellular-level lung injury induced by fluid mechanical stresses in microfluidic airway systems. Proc Natl Acad Sci. 2007;104(48):18886–91.
34. Huh D, Matthews BD, Mammoto A, Montoya-Zavala M, Hsin HY, Ingber DE. Reconstituting organ-level lung functions on a chip. Science. 2010;328(5986):1662–8.
35. Huh D, Leslie DC, Matthews BD, Fraser JP, Jurek S, Hamilton GA, et al. A human disease model of drug toxicity–induced pulmonary edema in a lung-on-a-chip microdevice. Sci Transl Med. 2012;4(159):159ra47.
36. Huh D, Kim HJ, Fraser JP, Shea DE, Khan M, Bahinski A, et al. Microfabrication of human organs-on-chips. Nat Protoc. 2013;8(11):2135–57.
37. Kim HJ, Huh D, Hamilton G, Ingber DE. Human gut-on-a-chip inhabited by microbial flora that experiences intestinal peristalsis-like motions and flow. Lab Chip. 2012;12(12):2165–74.
38. Kim HJ, Ingber DE. Gut-on-a-Chip microenvironment induces human intestinal cells to undergo villus differentiation. Integr Biol (Camb). 2013;5(9):1130–40.
39. Booth R, Kim H. Characterization of a microfluidic in vitro model of the blood-brain barrier ([small mu]BBB). Lab Chip. 2012;12(10):1784–92.
40. Griep LM, Wolbers F, de Wagenaar B, ter Braak PM, Weksler BB, Romero IA, et al. BBB on chip: microfluidic platform to mechanically and biochemically modulate blood-brain barrier function. Biomed Microdevices. 2013;15(1):145–50.
41. Achyuta AKH, Conway AJ, Crouse RB, Bannister EC, Lee RN, Katnik CP, et al. A modular approach to create a neurovascular unit-on-a-chip. Lab Chip. 2013;13(4):542–53.
42. Torisawa Y-s, Spina CS, Mammoto T, Mammoto A, Weaver JC, Tat T, et al. Bone marrow–on–a–chip replicates hematopoietic niche physiology in vitro. Nat Methods. 2014;11(6):663–9.
43. Jang KJ, Suh KY. A multi-layer microfluidic device for efficient culture and analysis of renal tubular cells. Lab Chip. 2010;10(1): 36–42.
44. Jang KJ, Cho HS, Kang do H, Bae WG, Kwon TH, Suh KY. Fluid-shear-stress-induced translocation of aquaporin-2 and reorganization of actin cytoskeleton in renal tubular epithelial cells. Integr Biol (Camb). 2011;3(2):134–41.

45.•• Jang KJ, Mehr AP, Hamilton GA, McPartlin LA, Chung S, Suh KY, et al. Human kidney proximal tubule-on-a-chip for drug transport and nephrotoxicity assessment. Integr Biol (Camb). 2013;5(9):1119–29. **This study utilizes a multilayer microfluidic system—comprised of two chambers separated by a thin, permeable membrane—to model functions of the proximal tubule for drug toxicity testing**.

46. Sciancalepore AG, Sallustio F, Girardo S, Gioia Passione L, Camposeo A, Mele E, et al. A bioartificial renal tubule device embedding human renal stem/progenitor cells. PLoS One. 2014;9(1):e87496.

47. Frohlich EM, Alonso JL, Borenstein JT, Zhang X, Arnaout MA, Charest JL. Topographically-patterned porous membranes in a microfluidic device as an in vitro model of renal reabsorptive barriers. Lab Chip. 2013;13(12):2311–9.

48. Ferrell N, Desai RR, Fleischman AJ, Roy S, Humes HD, Fissell WH. A microfluidic bioreactor with integrated transepithelial electrical resistance (TEER) measurement electrodes for evaluation of renal epithelial cells. Biotechnol Bioeng. 2010;107(4):707–16.

49. Olson H, Betton G, Robinson D, Thomas K, Monro A, Kolaja G, et al. Concordance of the toxicity of pharmaceuticals in humans and in animals. Regul Toxicol Pharmacol. 2000;32(1):56–67.

50. Greek R, Menache A. Systematic reviews of animal models: methodology versus epistemology. Int J Med Sci. 2013;10(3): 206–21.

51. Chu X, Bleasby K, Evers R. Species differences in drug transporters and implications for translating preclinical findings to humans. Expert Opin Drug Metab Toxicol. 2013;9(3):237–52.

52. Su R, Li Y, Zink D, Loo LH. Supervised prediction of drug-induced nephrotoxicity based on interleukin-6 and -8 expression levels. BMC Bioinformatics. 2014;15(16):S16.

53. Benam KH, Dauth S, Hassell B, Herland A, Jain A, Jang KJ, et al. Engineered in vitro disease models. Annu Rev Pathol. 2015;10: 195–262.

54. Lam AQ, Freedman BS, Bonventre JV. Directed differentiation of pluripotent stem cells to kidney cells. Semin Nephrol. 2014;34(4): 445–61.

55. Desrochers TM, Palma E, Kaplan DL. Tissue-engineered kidney disease models. Adv Drug Deliv Rev. 2014;69-70:67–80.

56. Huang HC, Chang YJ, Chen WC, Harn HI, Tang MJ, Wu CC. Enhancement of renal epithelial cell functions through microfluidic-based coculture with adipose-derived stem cells. Tissue Eng Part A. 2013;19(17-18):2024–34.

57. Zhou M, Ma H, Lin H, Qin J. Induction of epithelial-to-mesenchymal transition in proximal tubular epithelial cells on microfluidic devices. Biomaterials. 2014;35(5):1390–401.

58. Frohlich EM, Zhang X, Charest JL. The use of controlled surface topography and flow-induced shear stress to influence renal epithelial cell function. Integr Biol (Camb). 2012;4(1):75–83.

59. Wunsch S, Gekle M, Kersting U, Schuricht B, Oberleithner H. Phenotypically and karyotypically distinct Madin-Darby canine kidney cell clones respond differently to alkaline stress. J Cell Physiol. 1995;164(1):164–71.

60. Rose B, Post T. Introduction to renal function. Clinical physiology of acid-base and electrolyte disorders. New York: McGraw-Hill; 2001.

61. Abate AR, Lee D, Do T, Holtze C, Weitz DA. Glass coating for PDMS microfluidic channels by sol-gel methods. Lab Chip. 2008;8(4):516–8.

62.• Wei Z, Amponsah PK, Al-Shatti M, Nie Z, Bandyopadhyay BC. Engineering of polarized tubular structures in a microfluidic device to study calcium phosphate stone formation. Lab Chip. 2012;12(20):4037–40. **This work adapts conventional soft lithography methods (which produce rectangular microfluidic channels) to fabricate cylindrical microfluidic channels for investigating renal functions**.

63.• Oo ZY, Deng R, Hu M, Ni M, Kandasamy K, bin Ibrahim MS et al. The performance of primary human renal cells in hollow fiber bioreactors for bioartificial kidneys. Biomaterials. 2011;32(34): 8806-15. **The work presents a hollow, cylindrical fibrin-based permeable membrane for renal applications**.

64. Ng CP, Zhuang Y, Lin AWH, Teo JCM. A fibrin-based tissue-engineered renal proximal tubule for bioartificial kidney devices: development, characterization and in vitro transport study. Int J Tissue Eng. 2013;2013:10.

65. Tseng P, Murray C, Kim D, Di Carlo D. Research highlights: printing the future of microfabrication. Lab Chip. 2014;14(9): 1491–5.

66. Iwai K, Shih KC, Lin X, Brubaker TA, Sochol RD, Lin L. Finger-powered microfluidic systems using multilayer soft lithography and injection molding processes. Lab Chip. 2014;14(19):3790–9.

67. O'Neill PF, Ben Azouz A, Vázquez M, Liu J, Marczak S, Slouka Z, et al. Advances in three-dimensional rapid prototyping of microfluidic devices for biological applications. Biomicrofluidics. 2014;8(5):052112.

68. Kim JY, Baek JY, Lee KA, Lee SH. Automatic aligning and bonding system of PDMS layer for the fabrication of 3D microfluidic channels. Sensors Actuators A Phys. 2005;119(2):593–8.

69. Hull CW. Apparatus for production of three-dimensional objects by stereolithography. Google Patents; 1986.

70. Crump SS. Apparatus and method for creating three-dimensional objects. Google Patents; 1992.

71. Yamane M, Kawaguchi T, Kagayama S, Higashiyama S, Suzuki K, Sakai J et al. Apparatus and method for forming three-dimensional article. Google Patents; 1991.

72. Almquist TA, Smalley DR. Thermal stereolithography. Google Patents; 1997.

73. Lim TW, Son Y, Jeong YJ, Yang D-Y, Kong H-J, Lee K-S, et al. Three-dimensionally crossing manifold micro-mixer for fast mixing in a short channel length. Lab Chip. 2011;11(1):100–3.

74. He Y, Huang B-L, Lu D-X, Zhao J, Xu B-B, Zhang R, et al. "Overpass" at the junction of a crossed microchannel: an enabler for 3D microfluidic chips. Lab Chip. 2012;12(20):3866–9.

75. Shallan AI, Smejkal P, Corban M, Guijt RM, Breadmore MC. Cost-effective three-dimensional printing of visibly transparent microchips within minutes. Anal Chem. 2014;86(6):3124–30.

76. Bhargava KC, Thompson B, Malmstadt N. Discrete elements for 3D microfluidics. Proc Natl Acad Sci. 2014;111(42):15013–8.

77. Au AK, Lee W, Folch A. Mail-order microfluidics: evaluation of stereolithography for the production of microfluidic devices. Lab Chip. 2014;14(7):1294–301.

78. Au AK, Bhattacharjee N, Horowitz LF, Chang TC, Folch A. 3D-printed microfluidic automation. Lab Chip. 2015;15(8):1934–41.

79. Rogers CI, Qaderi K, Woolley AT, Nordin GP. 3D printed microfluidic devices with integrated valves. Biomicrofluidics. 2015;9(1):016501.

80. Zhang AP, Qu X, Soman P, Hribar KC, Lee JW, Chen S, et al. Rapid fabrication of complex 3D extracellular microenvironments by dynamic optical projection stereolithography. Adv Mater. 2012;24(31):4266–70.

81. Soman P, Kelber JA, Lee JW, Wright TN, Vecchio KS, Klemke RL, et al. Cancer cell migration within 3D layer-by-layer microfabricated photocrosslinked PEG scaffolds with tunable stiffness. Biomaterials. 2012;33(29):7064–70.

82. Hribar KC, Finlay D, Ma X, Qu X, Ondeck MG, Chung PH, et al. Nonlinear 3D projection printing of concave hydrogel microstructures for long-term multicellular spheroid and embryoid body culture. Lab Chip. 2015;15(11):2412–8.

83. Maruo S, Nakamura O, Kawata S. Three-dimensional microfabrication with two-photon-absorbed photopolymerization. Opt Lett. 1997;22(2):132–4.

84. Klein F, Striebel T, Fischer J, Jiang Z, Franz CM, von Freymann G, et al. Elastic fully three-dimensional microstructure scaffolds for cell force measurements. Adv Mater. 2010;22(8):868–71.
85.• Klein F, Richter B, Striebel T, Franz CM, Freymann G, Wegener M, et al. Two-component polymer scaffolds for controlled three-dimensional cell culture. Adv Mater. 2011;23(11):1341–5. **This study describes a two-photon DLW approach for constructing 3D cellular scaffolds comprised of distinct materials that either promote or limit cellular attachment at specified locations in 3D space**.
86. Scheiwe AC, Frank SC, Autenrieth TJ, Bastmeyer M, Wegener M. Subcellular stretch-induced cytoskeletal response of single fibroblasts within 3D designer scaffolds. Biomaterials. 2015;44:186–94.
87. Tumbleston JR, Shirvanyants D, Ermoshkin N, Janusziewicz R, Johnson AR, Kelly D, et al. Continuous liquid interface production of 3D objects. Science. 2015;347(6228):1349–52.
88. Therriault D, White SR, Lewis JA. Chaotic mixing in three-dimensional microvascular networks fabricated by direct-write assembly. Nat Mater. 2003;2(4):265–71.
89. Ahn BY, Duoss EB, Motala MJ, Guo X, Park S-I, Xiong Y, et al. Omnidirectional printing of flexible, stretchable, and spanning silver microelectrodes. Science. 2009;323(5921):1590–3.
90. Wu W, DeConinck A, Lewis JA. Omnidirectional printing of 3D microvascular networks. Adv Mater. 2011;23(24):H178–83.
91. Miller JS, Stevens KR, Yang MT, Baker BM, Nguyen D-HT, Cohen DM, et al. Rapid casting of patterned vascular networks for perfusable engineered three-dimensional tissues. Nat Mater. 2012;11(9):768–74.
92. Derby B. Printing and prototyping of tissues and scaffolds. Science. 2012;338(6109):921–6.
93. Onoe H, Okitsu T, Itou A, Kato-Negishi M, Gojo R, Kiriya D, et al. Metre-long cell-laden microfibres exhibit tissue morphologies and functions. Nat Mater. 2013;12(6):584–90.
94. Rutz AL, Hyland KE, Jakus AE, Burghardt WR, Shah RN. A multimaterial bioink method for 3D printing tunable, cell-compatible hydrogels. Adv Mater. 2015;27(9):1607–14.
95. Gao Q, He Y, Fu J-z, Liu A, Ma L. Coaxial nozzle-assisted 3D bioprinting with built-in microchannels for nutrients delivery. Biomaterials. 2015;61:203–15.
96.•• Kolesky DB, Truby RL, Gladman AS, Busbee TA, Homan KA, Lewis JA. 3D bioprinting of vascularized, heterogeneous cell-laden tissue constructs. Adv Mater. 2014;26(19):3124–30. **This work combines two distinct extrusion-based 3D bioprinting approaches—sacrifical casting and direct deposition of cell-laden inks—to enable interactions between multiple cell types and microvascular networks**.
97. Anderson KB, Lockwood SY, Martin RS, Spence DM. A 3D printed fluidic device that enables integrated features. Anal Chem. 2013;85(12):5622–6.
98. Lee KG, Park KJ, Seok S, Shin S, Kim DH, Park JY, et al. 3D printed modules for integrated microfluidic devices. RSC Adv. 2014;4(62):32876–80.
99. Walczak R, Adamski K. Inkjet 3D printing of microfluidic structures—on the selection of the printer towards printing your own microfluidic chips. J Micromech Microeng. 2015;25(8):085013.
100. Zhu F, Skommer J, Macdonald NP, Friedrich T, Kaslin J, Wlodkowic D. Three-dimensional printed millifluidic devices for zebrafish embryo tests. Biomicrofluidics. 2015;9(4):046502.